Article

Olefin Metathesis in Confined Geometries: A Biomimetic Approach Towards Selective Macrocyclization

Felix Ziegler, Johannes Teske, Iris Elser, Michael Dyballa, Wolfgang Frey, Hamzeh Kraus, Niels Hansen, Julia Rybka, Ulrich Tallarek, and Michael R Buchmeiser

J. Am. Chem. Soc., **Just Accepted Manuscript** • DOI: 10.1021/jacs.9b08776 • Publication Date (Web): 07 Nov 2019

Olefin Metathesis in Confined Geometries: A Biomimetic Approach Towards Selective Macrocyclization

Felix Ziegler[†], Johannes Teske[†], Iris Elser[†], Michael Dyballa[‡], Wolfgang Frey[§], Hamzeh Kraus[∥], Niels Hansen[∥], Julia Rybka[⊥], Ulrich Tallarek[⊥], Michael R. Buchmeiser*[†]

[†]Institute of Polymer Chemistry, [‡]Institute of Chemical Technology, [§]Institute of Organic Chemistry, University of Stuttgart, Pfaffenwaldring 55, D-70569 Stuttgart, Germany

[∥]Institute of Thermodynamics and Thermal Process Engineering, University of Stuttgart, Pfaffenwaldring 9, D-70569 Stuttgart, Germany

[⊥]Department of Chemistry, Philipps-University of Marburg, Hans-Meerwein-Strasse 4, D-35032 Marburg, Germany

ABSTRACT: The synthesis of macrocycles is severely impeded by concomitant oligomer formation. Here, we present a biomimetic approach that utilizes spatial confinement to increase macrocyclization selectivity in the ring closing metathesis of various dienes at elevated substrate concentration up to 25 mM using an olefin metathesis catalyst selectively immobilized inside ordered mesoporous silicas with defined pore diameters. By this approach, the ratio between macro(mono)cyclization (MMC) product and all undesired oligomerization products (O) resulting from acyclic diene metathesis polymerization was increased from 0.55, corresponding to 35% MMC product obtained with the homogeneous catalyst, up to 1.49, corresponding to 60% MMC product. A correlation between the MMC/O ratio and the substrate-to-pore-size ratio was successfully established. Modification of the inner pore surface with dimethyldimethoxysilane allowed to fine-tune the effective pore size and to reverse surface polarity, which resulted in a further increase of the MMC/O ratio up to 2.2, corresponding to > 68% MMC product. Molecular-level simulations in model pore geometries help to rationalize the complex interplay between spatial confinement, specific (substrate and product) interaction with the pore surface, and diffusive transport. These effects can be synergistically adjusted for optimum selectivity by suitable surface modification.

INTRODUCTION

Macrocyclic compounds play an important role in pharmaceutical chemistry, e.g., as fragrances and drugs.[1-2] Macrocyclization can be accomplished by different means,[3] however, catalytic reactions such as olefin metathesis have moved into the focus,[4-11] the more since these reactions can nowadays be realized with high stereoselectivity.[12-15] An unsolved problem in macrocyclization is related to the efficiency of this type of reaction. Mostly for entropic reasons, oligomerization often dominates over macrocyclization. In fact, Fogg et al.[16] clearly demonstrated that ring-closing metathesis (RCM) does not selectively proceed via cyclization of the substrate as such, but also involves oligomerization followed by back-biting and concomitant RCM. In other words, if olefin metathesis is used for macrocyclization, RCM and acyclic diene metathesis (ADMET) oligomerization compete to a substantial extent, leading to low macro(mono)cyclization (MMC) yields because of the ring-chain equilibrium (Scheme 1).[16-17] This is particularly unfavorable in case the starting diene has been prepared through a multi-step, possibly stereoselective synthesis, as is often the case with many progenitors for biologically and pharmaceutically active compounds. One approach to improve macrocyclization yields entails highly dilute conditions, typically ≤ 5 mM in substrate.[18-20] Furthermore, the slow addition of the substrate to a catalyst solution promotes RCM.[3, 15] With cyclic ethers this problem can be alleviated by the use of Li-ions,[21-23] which form cyclic chelates and thus favor macrocyclization over oligomerization. Recently, Fogg et al.[24] outlined the use of an *N,N*-chelated Ru-alkylidene, which allowed for high macrocyclization yields, albeit still at 1 mol-% catalyst and 0.5 mM substrate levels. Grela et al.[25] used the back-biting reaction in combination with a tailored distillation apparatus to constantly remove the macrocyclic product. This way it was possible to work at higher substrate concentration (up to 0.2 M) at a 1 mol-% catalyst

level. However, this strategy is obviously restricted to macrocyclization products that can be readily distilled and also requires significant differences in the boiling points of the starting compound and the product. Immobilization strategies[26] have been used, too, to improve macrocyclization yields.[27-28] Unfortunately, these again required low substrate concentrations (0.5 mM) as well as high catalyst loadings (5 mol-%). Also, immobilization has often been accomplished via the alkylidene moiety, which releases the catalyst during the first catalytic cycle, impedes permanent immobilization and makes continuous flow experiments impossible.[29] Similar accounts for physisorbed catalysts.[30] Consequently, compared to the homogeneous catalyst, improved macrocyclization selectivity was only achieved in very few cases. Finally, cavitands have been reported to favor RCM-based macrocyclization, though again at low substrate concentration and high catalyst loading (3 mol-%).[31]

Here, we present a new biomimetic approach that uses a biological concept to eliminate the drawbacks related to macrocyclization to a great extent and which allows running macrocyclization reactions at low catalyst loading and higher substrate concentration. Similar to enzymes, which can create highly substrate specific reaction sites, our concept is based on the idea to synergistically use both a well-defined organometallic catalyst and a defined pore shape and size to create chemoselective reaction sites through spatial confinement. The underlying concept entails the pore size selective immobilization of a ruthenium-based olefin metathesis catalyst inside the pores of a support, here SBA-15-type silica, which is a mesoporous silica consisting of ordered, hexagonally arranged, cylindrical pores.[32-33] Similar to an enzyme or a metalloenzyme,[34-36] this particular approach provides a confined space for the macrocyclization reaction. If the pore diameter is tuned such that only one substrate can approach the catalyst inside the pore at the same time, MMC must prevail and oligomerization be suppressed (Scheme 1).

Scheme 1. Concept of macrocyclization in confined geometries.

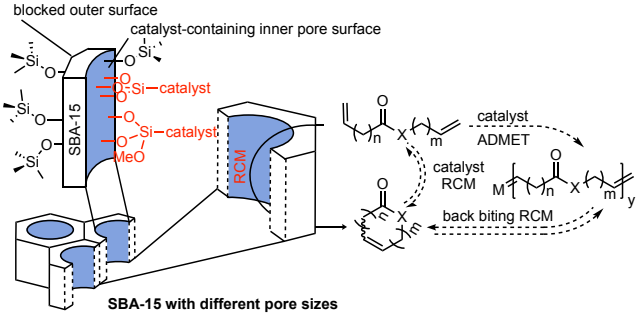

Importantly, this concept can only be expected to work if the catalyst is selectively fixed *inside* but not *outside* the mesopores and the hydrodynamic diameter of the substrate fits the pore diameter. This, in turn, requires a pore size-selective functionalization and careful tuning of the pore diameter. According to the study of hindered diffusion in similar ordered mesoporous silicas by Tallarek *et al.*[37] the hydrodynamic diameter of both the catalyst and the substrate should be less than ca. one third of the nominal pore diameter, since otherwise diffusion into the pores becomes severely obstructed.

RESULTS AND DISCUSSION

Scheme 2 illustrates the synthesis of the homogeneous catalyst bearing a trimethoxysilyl-tether at the NHC, which was used for its immobilization on the silica support. Mesitylimidazole was reacted with (3-iodopropyl)trimethoxysilane to yield the 1,3-disubstituted imidazolium salt, which was then deprotonated with potassium hexamethyldisilazide (HMDS). The resulting free carbene was finally reacted with the 1st-generation Grubbs-Hoveyda catalyst to yield catalyst **3**.

Scheme 2. Synthesis of catalyst 3.

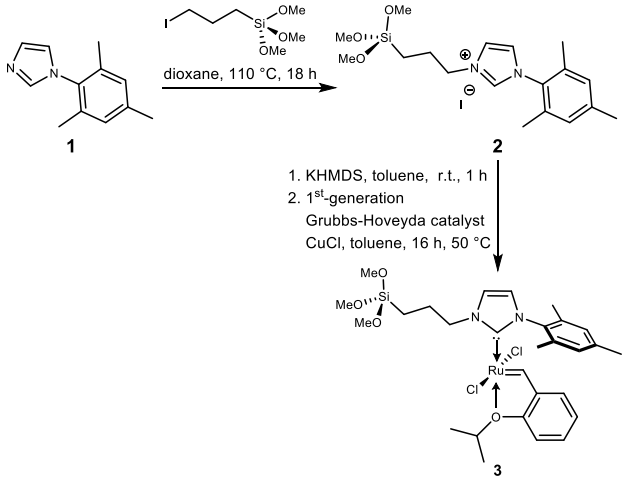

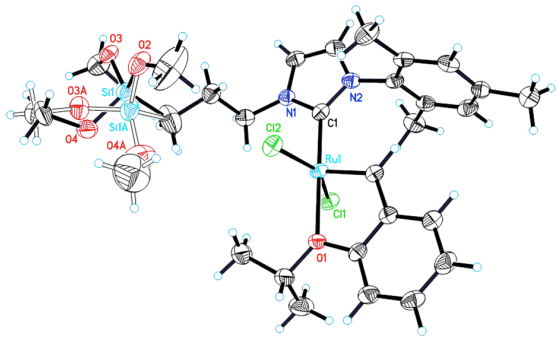

Figure 1. Single crystal X-ray structure of **3**. Selected bond lengths [pm] and angles [°]: Ru(1)-C(19) 182.9(5); Ru(1)-C(1) 199.8(5); Ru(1)-O(1) 225.8(3); Ru(1)-Cl(1) 233.13(13); Ru(1)-Cl(2) 233.21(13); C(19)-Ru(1)-Cl(2)

104.98(14); C(19)-Ru(1)-O(1), 101.0(2); C(1)-Ru(1)-Cl(1) 90.18(13); C(1)-Ru(1)-Cl(2) 92.29(13); C(1)-Ru(1)-O(1) 178.33(15); O(1)-Ru(1)-Cl(1) 88.15(9); O(1)-Ru(1)-Cl(2) 89.21(9); Cl(1)-Ru(1)-Cl(2) 152.52(5).

Notably, catalyst **3** is stable under air. Figure 1 shows its single crystal X-ray structure along with selected bond lengths and angles. **3** crystallizes in a monoclinic system in the space group P21/c (a = 1268.39(7) pm, b = 2797.40(14) pm, c = 952.88(5) pm; $\alpha = \gamma = 90°$ and $\beta = 108.741(2)$). All bond lengths and angles are unsuspicious; all methoxy-groups are distorted.

Two different silica materials with defined average pore diameters of 50 Å and 62 Å, respectively, referred to as **SBA-15$_{50Å}$** and **SBA-15$_{62Å}$**, were modified to allow for a selective catalyst immobilization inside the mesopores (Scheme 3). Ruthenium, i.e., catalyst loadings determined by ICP-OES were 2.0 and 3.4 µmol/g for **3 @ SBA-15$_{50Å}$** and **3 @ SBA-15$_{62Å}$**, respectively. To confirm pore-selective catalyst immobilization, we also immobilized **3** on both unmodified SBA 15$_{50Å}$ and SBA-15$_{62Å}$, referred to as **SBA-15$_{50Å\ unmodified}$** and **SBA-15$_{62Å\ unmodified}$**. A comparison between **3 @ SBA 15$_{50Å}$/SBA 15$_{62Å}$** and **3 @ SBA 15$_{50Å\ unmodified}$/SBA-15$_{62Å\ unmodified}$** revealed Ru-loadings of 2.0/3.4 and 40.5/56.0 µmol/g, respectively. The low Ru-loading in modified SBA-15 suggests that the majority of **3** is indeed located inside but not outside the mesopores. Energy-dispersive X-ray (EDX) spectroscopy measurements were carried out and proved the existence of catalyst on unmodified SBA-15 (Figure S6 and Figure S7); however, the Ru-loading on modified SBA-15 was too low to be measured. We make a diffusion-controlled immobilization accountable for the comparatively low catalyst loadings in the modified SBAs.

Scheme 3. Multi-step modification[38] of SBA-15 for pore-selective immobilization of the catalyst inside the mesopores.

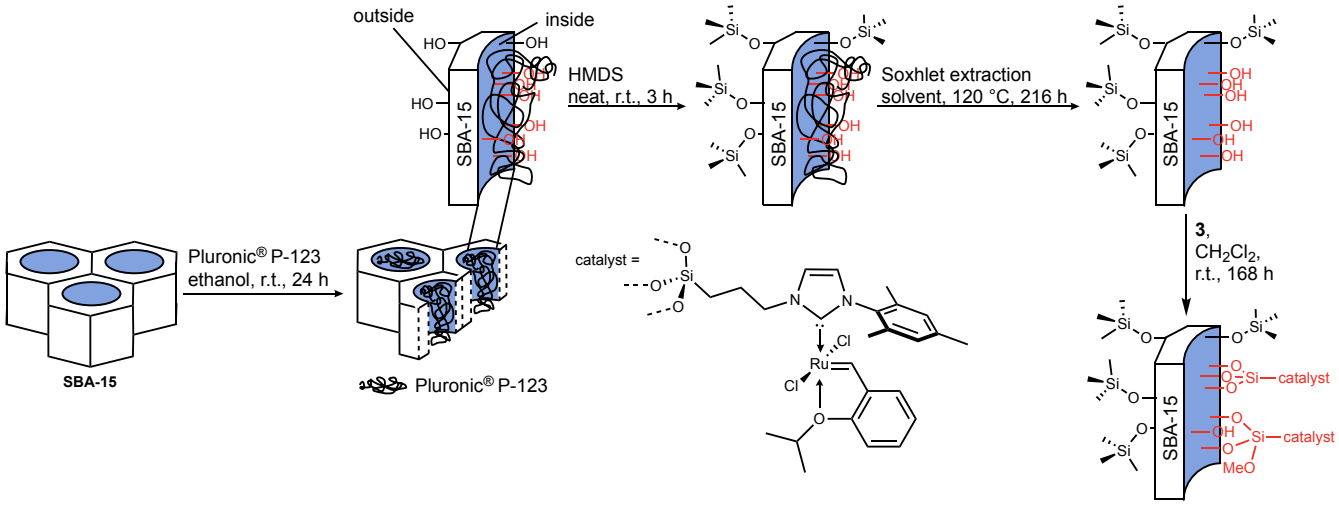

By contrast, the higher loadings observed with unmodified SBA stem from catalyst immobilization both outside and inside the pores.

We then evaluated the selectivity of **3 @ SBA-15$_{50Å}$** and **3 @ SBA-15$_{62Å}$** along with the homogeneous catalyst for a number of substrates characterized by different hydrodynamic diameters and functional groups (Figure 2 and Scheme 4). Using 0.1 mol-% catalyst, conversion was between 15 and 55%. Compared to the homogeneous catalyst, macrocyclization selectivity was substantially improved for all substrates with both materials. **3 @ SBA-15$_{50Å}$** exhibited the highest selectivity of 66% (MMC/O = 1.94 for substrate **5**) at substantially elevated substrate concentration of 25 mM (Figure 3). The determination of the MMC:O ratios by NMR is exemplified for substrate **5**. One needs to integrate the signal of the oligomer (O) around 5.520 ppm and the signals for both the *E*- and *Z*-monomacrocycle (MMC) at 5.457 ppm and 5.429 ppm (see Figure S9). Generally, a higher macrocyclization selectivity was observed with larger substrates, at similar conversion, when using **3 @ SBA-15$_{50Å}$** instead of **3 @ SBA-15$_{62Å}$** (Figure 3). This strongly suggests that a confinement effect based on the size of the substrate and of the pore is effective. By upscaling the RCM reaction of substrate **5** with **3 @ SBA-15$_{50Å}$** (MMC/O = 1.97) by a factor of 25 it could be shown that it is also possible to work with larger quantities (Table S8).

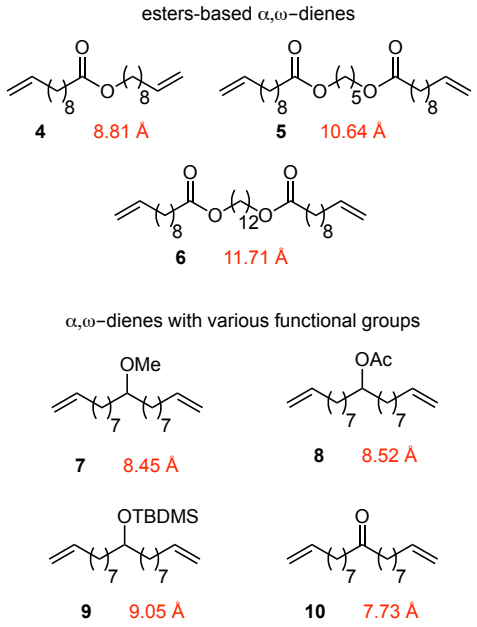

Figure 2. Various α,ω-dienes used in macrocyclization. Hydrodynamic diameter (in red) as determined via DOSY-NMR in deuterated benzene using the Stokes-Einstein equation.

Scheme 4. Examples for the reaction of substrates 5 and 9 with 3 @ SBA-15$_{50Å}$, 3 @ SBA-15$_{50Å\text{-}DMDMS}$, 3 @ SBA-15$_{62Å}$, and 3 @ SBA-15$_{62Å\text{-}DMDMS}$, and with the homogeneous catalyst 3 to the macro(mono)cyclization products 11 and 12.

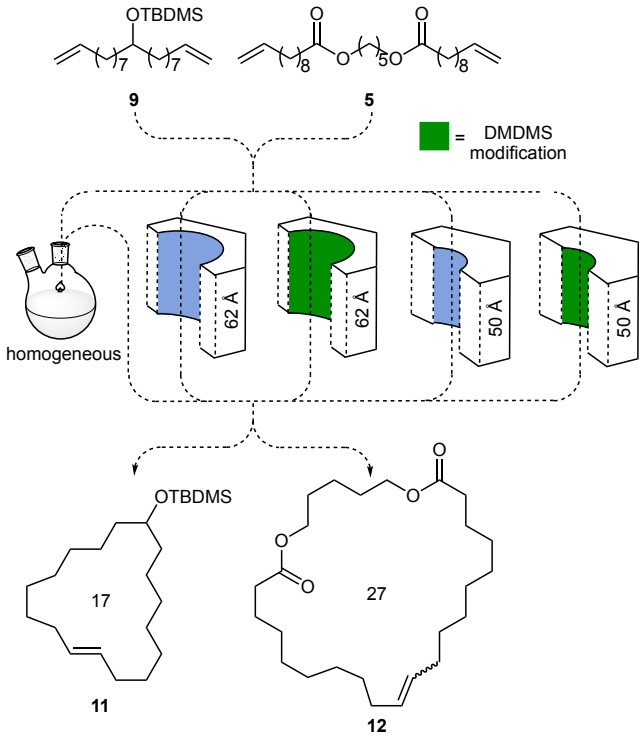

To reduce the pore size and reverse the pore surface polarity, we additionally modified the inner surface of the SBA-15 materials after immobilization of the catalyst with dimethoxydimethylsilane (DMDMS). This modification further increased selectivity as demonstrated for substrates **4**–**6** and **8**–**10** (Figure 4). In the case of **9**, macrocyclization selectivity increased from MMC/O = 0.55 to 1.80 for **3 @ SBA-15$_{50Å\text{-}DMDMS}$** as compared to **3** operating in solution. This corresponds to an increase in macrocyclization selectivity of 29% with respect to **3** operating in solution (Figure 5). Indeed, with the macrocyclization selectivity for the homogeneous catalyst **3** as reference (100%), a plot of selectivity changes for the individual substrates against their hydrodynamic diameter reveals a clear trend for **SBA-15$_{50Å}$** (Figure 5). Up to a hydrodynamic diameter of ~0.9 nm the selectivity increases irrespective of the functional group of the substrate, while above ~0.9 nm MMC selectivity drops quickly.

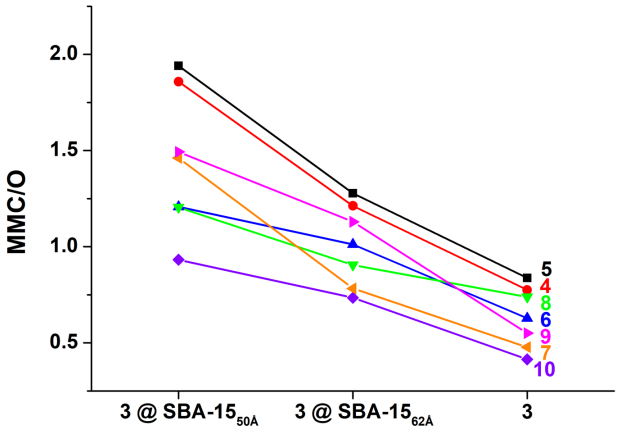

Figure 3. MMC/O ratios obtained in the RCM of substrates 4–10 using **3 @ SBA-15$_{50Å}$** or **SBA-15$_{62Å}$** and with the homogeneous catalyst 3. Reactions were run for 24 hours in C6D6 at 50 °C, using 0.1 mol-% catalyst with respect to substrate and a 25 mM substrate concentration.

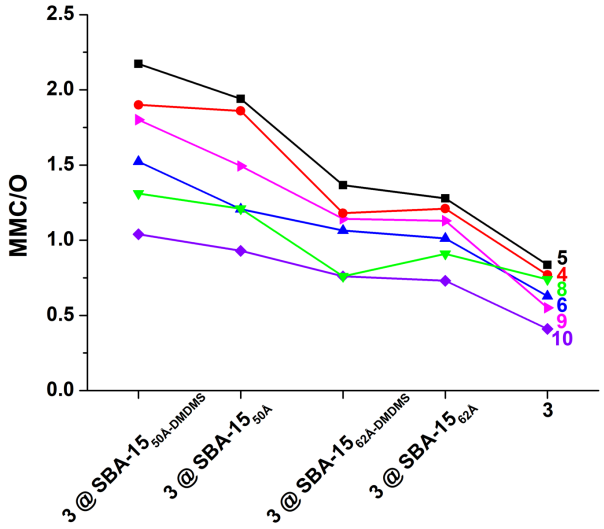

Figure 4. MMC/O ratios for the reaction of **3 @ SBA-15$_{50Å}$**, **3 @ SBA-15$_{50Å\text{-}DMDMS}$**, **3 @ SBA-15$_{62Å}$**, **3 @ SBA-15$_{62Å\text{-}DMDMS}$** and the homogeneous catalyst **3** obtained in the RCM of substrates **4**–**6** and **8**–**10** in C_6D_6 after 24 hours

at 50 °C using 0.1 mol-% of catalyst with respect to substrate and 25 mM substrate concentration.

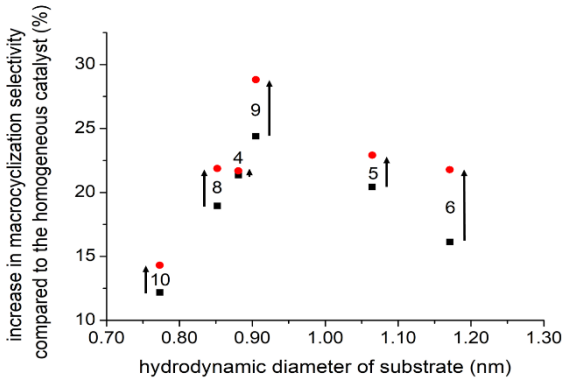

Figure 5. Results in Figure 3 and Figure 4 for **3 @ SBA-15$_{50Å}$** were plotted against the hydrodynamic diameter of substrates **4**–**6** and **8**–**10** (black). The results for **3 @ SBA-15$_{50Å\text{-}DMDMS}$** are plotted against the hydrodynamic diameter of substrates **4**–**6**, and **8**–**10** (red). Arrows indicate the increase in macrocyclization selectivity between **3 @ SBA-15$_{50Å}$** and **3 @ SBA-15$_{50Å\text{-}DMDMS}$**.

In that regards, macrocyclization efficiency serves as probe for the confinement effect. Indeed, it highlights the enzyme-like sensitivity, with which the spatial confinement affects macrocyclization, identifying just a narrow operational window for optimum MMC selectivity. Furthermore, the systematically higher selectivity observed for **3 @ SBA-15$_{50Å\text{-}DMDMS}$** is attributed to both the reduced pore diameter *and* the weakened interaction between the nonpolar surface and the ester, ether, or carbonyl groups of the products, which supposedly results in shorter residence times at and near the catalytic centers and, thus, in a reduced probability of the macrocycles to experience ring reopening (cf. Scheme 1). Indeed, the DMDMS-modification actually reverses the surface polarity from polar to nonpolar. Since most substrates are highly nonpolar, pore polarity must play an important role in substrate transport into and out of the pores. This effect is clearly mirrored by the results. Thus, the increase in macrocyclization selectivity (Figure 5, arrows) is stronger for the more nonpolar substrates **6** and **9** than for the more polar ones (e.g., **4** and **10**).

To better understand the important fine-tuning effects of the chemical surface modification, which add to the basic morphological properties of the underlying SBA-15 support (pore size, shape, and connectivity), we utilized molecular dynamics simulations employing cylindrical model pore geometries with and without DMDMS-modification. Figure 6a,b depict front and side view, respectively, onto the ~4.8 nm-diameter, 10 nm-long model silica pore with DMDMS groups and two catalytic centers **3** at its inner surface (Figure 6a). The solvent benzene contains equimolar amounts of substrate **5** and product **12**, which are distributing between the two pore-flanking reservoirs and the pore (Figure 6b). The radial profiles of substrate and product (density distributions) in the unmodified (Figure 6c) and the DMDMS-modified pore (Figure 6d) reveal substantial differences that are engendered by the surface modification: In the unmodified pore, both substrate and product molecules strongly enrich near the surface due to localized adsorption with their carbonyl oxygen onto the silanol groups of the bare silica surface via hydrogen bonding. This is reflected by the yellow and orange lines in Figure 6c, which peak close to the surface. The hydrophobic tails of the molecules are oriented towards the pore center, away from the polar surface (blue and green lines). In the DMDMS-modified pore (Figure 6d), by contrast, the enrichment of substrate and product molecules along the surface with its now reversed polarity is essentially suppressed (note the order of magnitude difference in the density scales in Figure 6c and d and, consequently, the molecules are more uniformly distributed over the pore cross-section. To verify the impact of the strikingly different adsorption behavior on pore-level transport of substrate and product molecules, we first recorded their diffusion profiles in the unmodified and the DMDMS-modified pore (Figure 6e). Due to the lack of adsorption onto (or even partitioning into) the DMDMS layer, diffusion near the nonpolar surface is enhanced compared to the unmodified bare-silica pore, where the localized adsorption onto the silanol groups significantly slows down molecular transport near the surface. Together with the radial density distributions $\rho(r)$ shown in Figure 6c,d, the radial profiles of the diffusion coefficients parallel to the pore axis $D_{||}(r)$ in Figure 6e can, in turn, be used to calculate average pore diffusivities of substrate and product molecules according to

$$\langle D_{||} \rangle = \frac{\int \rho(r) D_{||}(r) r dr}{\int \rho(r) r dr} \qquad (1)$$

in which r is the radial distance from the pore center. In the unmodified pore, we obtained diffusivities according to eq. (1) of 0.23×10^{-9} m^2s^{-1} (substrate) and 0.25×10^{-9} m^2s^{-1} (product). For the DMDMS-modified pore, they strongly increase to 0.71×10^{-9} m^2s^{-1} (substrate) and 0.73×10^{-9} m^2s^{-1} (product), that is, by a factor of three.

There are several implications emerging from the results in Figure 6. Local enrichment of substrate and product molecules near the catalytic centers is unfavorable since it increases the risk of both oligomerization (proximity of substrate molecules) and backbiting (proximity of product molecules). Suitable surface modification suppresses the adsorption and local enrichment, leading to higher pore-level diffusivities that guarantee faster transport of substrate molecules

to (and product molecules from) the catalytic centers, and furthermore enhances the confinement effect. This interplay of effects introduced by the surface modification rationalizes the improved MMC selectivity seen in the experiments and can also form the basis for optimizing the conversion by reducing transport limitations.

However, due to catalyst decomposition and diffusion limitations in the SBA-15 particles under the experimental conditions, conversions are generally lower for **3** immobilized on any SBA-15 material than for the homogeneous catalyst. Accordingly, **3 @ SBA-15$_{50Å}$** always showed the lowest conversion for all substrates. However, the reaction kinetics of substrate **5** recorded with **3 @ SBA-15$_{50Å}$** and **3 @ SBA-15$_{62Å}$** and for the homogeneous catalyst **3** (Figure 7a) revealed that macrocyclization selectivity remained virtually independent of conversion with MMC/O = 1.91, 1.41, and 0.83 for **3 @ SBA-15$_{50Å}$**, **3 @ SBA-15$_{62Å}$**, and the homogeneous catalyst **3**, respectively. The diffusion-limited intraparticle transport and catalyst decomposition also caused the substrate conversion to deviate from a 1st-order reaction kinetics. In view of these results, different reaction temperatures were investigated (Figure 7b). With increasing temperature, both conversion and selectivity increased for **3 @ SBA-15$_{50Å}$** and **3 @ SBA-15$_{62Å}$** (MMC/O = 1.63, 2.26, 1.15, and 1.64 for **3 @ SBA-15$_{50Å}$ @** 10 °C, **3 @ SBA-15$_{50Å}$ @** 70 °C, **3 @ SBA-15$_{62Å}$ @** 10 °C, and **3 @ SBA-15$_{62Å}$ @** 70 °C, respectively). The higher temperatures result in lower viscosities of the reaction mixture and thus in faster diffusion to and from the catalyst, which explains the higher conversion. In addition, the reaction should be accelerated due to a reduced stability of all ruthenacyclobutane intermediates.[39-42] On the other hand, higher temperatures reduce the extent of substrate and product adsorption onto the surface (an issue highlighted in Figure 6) and therefore also account for the increased MMC selectivity. When performing the RCM reaction at different substrate concentrations and catalyst:substrate ratios (Figure 7c,d), it becomes evident that even small amounts of **3** immobilized at the pore entrances to the SBA-15 particles suffice to adversely affect selectivity such that the spatial confinement effect offered by the mesopores cannot be fully exploited. In principle, **3 @ SBA-15$_{50Å}$** or **3 @ SBA-15$_{62Å}$** should not show any decrease in selectivity with higher substrate concentration (Figure 7c, right panel) provided that all catalysts experience a perfect confinement effect.

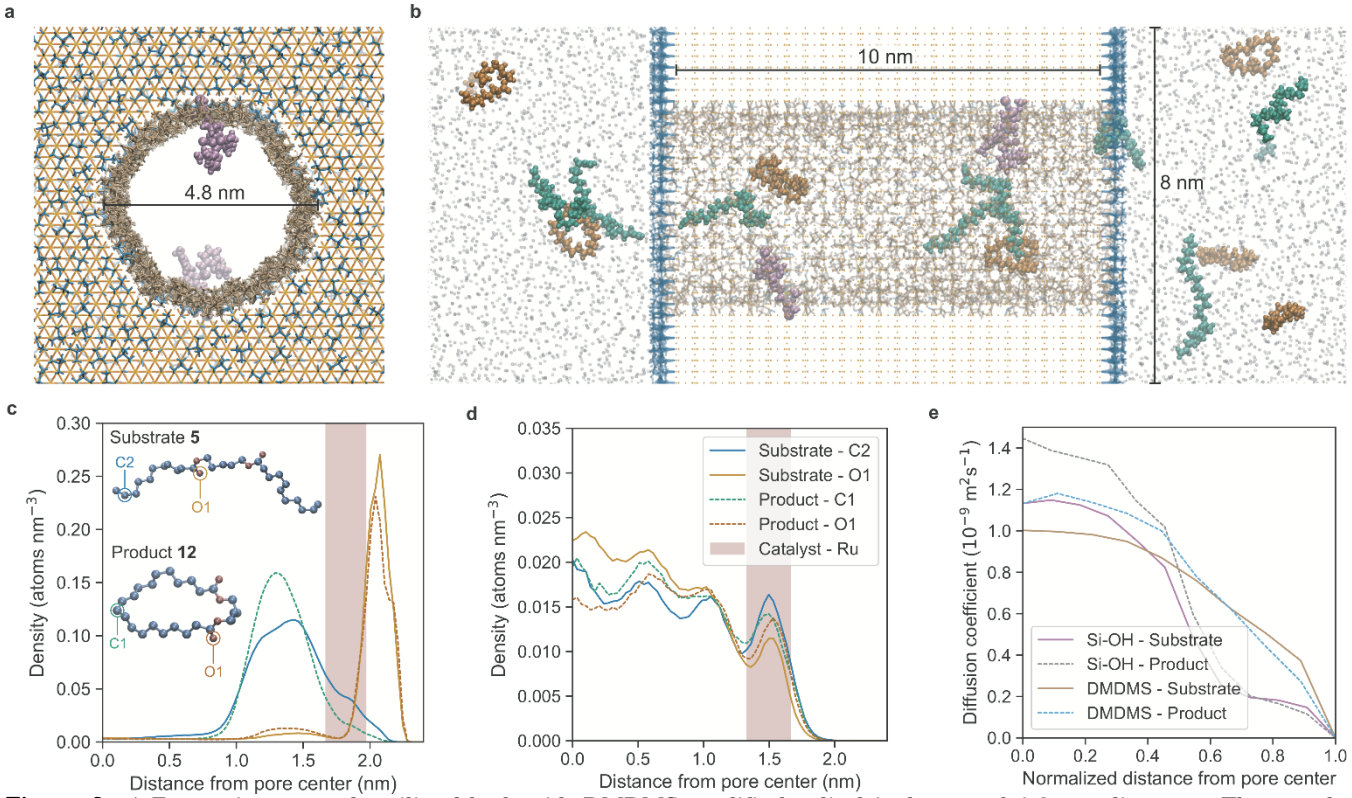

Figure 6. a) Front view onto the silica block with DMDMS-modified cylindrical pore of 4.8 nm diameter. The purple structures represent two catalysts **3** attached to the inner pore surface. b) Side view of the simulation box with equimolar amounts of substrate **5** (green) and product **12** molecules (orange). The pierced silica block is flanked by two solvent reservoirs. Benzene as the solvent is indicated by the grey dots. c) Radial number density profiles of the carbonyl

oxygen (yellow/orange) and vinylic carbon (blue/green) in the substrate (solid lines) and product (dashed lines), respectively, in the unmodified pore. The shaded area indicates the configurational space accessible by the ruthenium atom of the catalyst. d) Distributions corresponding to panel c, but in the DMDMS-modified pore. e) Radial dependence of the axial self-diffusion coefficient of substrate (solid lines) and product molecules (dashed lines) in the unmodified (pink and gray) and the DMDMS-modified pore (brown and cyan). The radial distance r from the pore center (where $r = 0$) is normalized by the effective pore radius, representing the region accessible to the substrate and product molecules.

However, once even small amounts of **3** are located close to the entrance of a pore leading into an SBA-15 particle, the fraction of substrate molecules that react with the catalyst at the pore entrance must be higher at low catalyst:substrate ratio. Indeed, an almost exponential loss in macrocyclization selectivity was observed for **3 @ SBA-15$_{50Å}$** and **3 @ SBA-15$_{62Å}$** with increasing catalyst:substrate ratio (MMC/O = 2.12, 1.48, 1.76, and 1.05 for **3 @ SBA-15$_{50Å}$** @ 0.05 mol-%, **3 @ SBA-15$_{50Å}$** @ 0.4 mol-%, **3 @ SBA-15$_{62Å}$** @ 0.05 mol-%, and **3 @ SBA-15$_{62Å}$** @ 0.4 mol-%) (Figure 7d). Clearly, with a maximum turnover number for each catalytic center prior to decomposition, low catalyst:substrate ratios make it more likely that catalysts located further inside the pore (and particle) react. While these findings are consistent with the proposed confinement effect, they do not adversely affect the practical implementation of this approach, since RCM reactions are usually carried out with the lowest possible catalyst:substrate ratio. In line with our findings and explanations, the homogeneous catalyst **3** showed (within experimental error) the expected, slightly increasing macrocyclization selectivity over the investigated range of catalyst:substrate ratios with respect to substrate **5** (MMC/O = 0.85 and 0.88 for 0.05 and 0.4 mol-% of **3**, cf. Figure 7d).

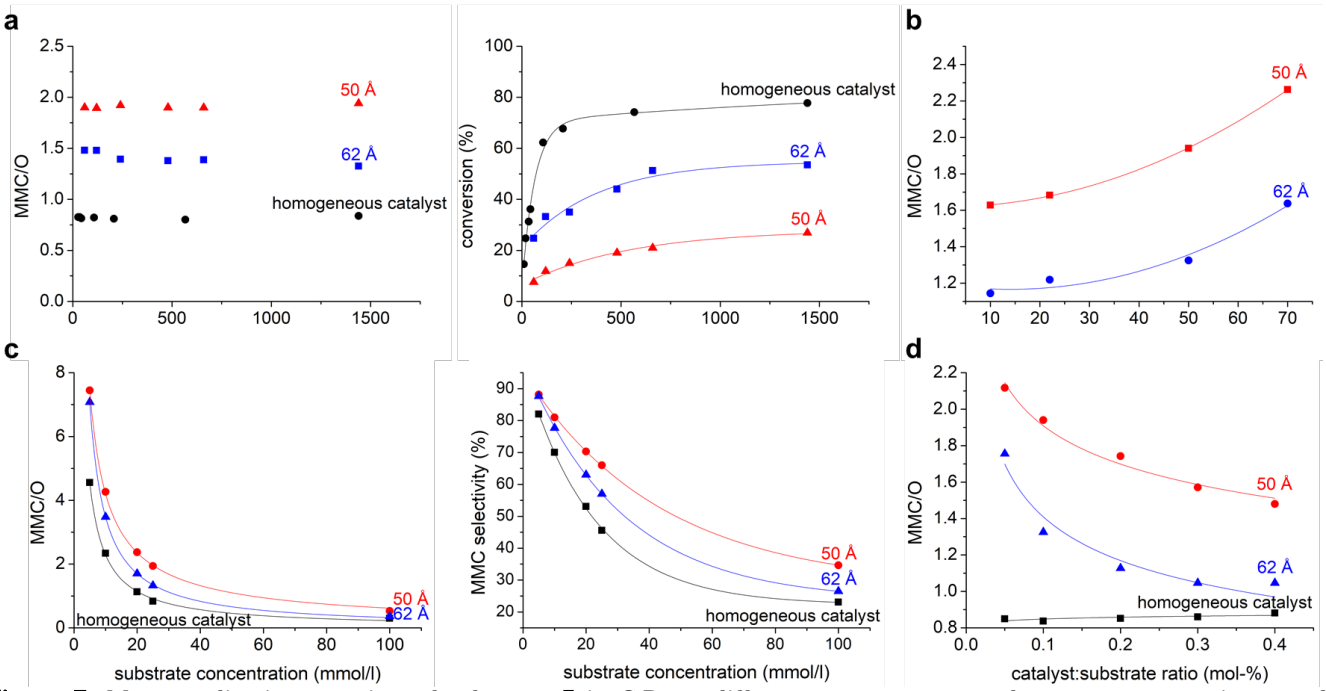

Figure 7. Macrocyclization reaction of substrate **5** in C_6D_6 at different temperatures, substrate concentrations, and catalyst:substrate ratios. a) Macrocyclization kinetics for **5** with **3 @ SBA-15$_{50Å}$** and **3 @ SBA-15$_{62Å}$** and with the homogeneous catalyst **3** at 25 mM substrate concentration and 0.1 mol-% catalyst:substrate ratio. In the case of **3 @ SBA-15$_{50Å}$** and **3 @ SBA-15$_{62Å}$**, each point represents a new reaction terminated at different times. Macrocyclization of **5** with **3 @ SBA-15$_{50Å}$** and **3 @ SBA-15$_{62Å}$** and with the homogeneous catalyst **3** at b) different temperatures (10, 24, 50, and 70 °C; catalyst:substrate ratio: 0.1 mol-%; substrate concentration: 25 mM), c) different substrate concentrations (5, 10, 20, and 25 mM; catalyst:substrate ratio: 0.1 mol-%; temperature: 50 °C), and d) different catalyst:substrate ratios (0.05, 0.1, 0.2, 0.3, and 0.4 mol-%; substrate concentration: 25 mM; 50 °C).

EXPERIMENTAL SECTION

General procedure for the synthesis of esters-based α,ω-dienes (GP-1). To a stirred solution of the acid chloride (21.0 mmol) in CH_2Cl_2 (40 mL) was subsequently added pyridine (1.7 mL, 21.0 mmol) and the corresponding alcohol (9.5 mmol/19 mmol) at 0 °C.

After stirring for 4 hours at room temperature, the reaction mixture was washed with 1.0 M aq. HCl solution (40 mL), sat. aq. $NaHCO_3$ solution (40 mL), brine (40 mL), dried over anhydrous Na_2SO_4, filtered, and evaporated. The obtained crude product was purified via column chromatography on SiO_2 to obtain the corresponding ester.

General Procedure for the RCM of α,ω-dienes (GP-2). To a stirred solution of the diene (0.75 mmol) in CH_2Cl_2 (200 mL) was added the 2nd-generation Grubbs catalyst (31.8 mg, 0.0375 mmol, 5 mol-%) at room temperature. After stirring for 14 hours under reflux and under N_2, the reaction mixture was cooled to room temperature and ethyl vinyl ether (5 mL, 70 eq) was added. The mixture was stirred for further 2 hours at room temperature. All volatiles were removed under reduced pressure, the obtained crude product was purified via column chromatography on SiO_2 to obtain the corresponding macrocyclic product, whose (E)/(Z) isomers were separated by semi-preparative HPLC.

General procedure for the RCM of α,ω-dienes with 3 (GP-3). The substrate was dissolved in C_6D_6 (990.5 µL) and the catalyst **3** (stock solution 9.5 µL) was added. After 24 hours, ^{1}H NMR data were acquired. The conversion and the ratio of macro(mono)cyclization (MMC) to oligomerization (O) were determined by integration of the corresponding signals.

General procedure for the RCM of α,ω-dienes with 3 @ SBA-15 (GP-4). The substrate was dissolved in C_6D_6 (1.0 mL) and the corresponding SBA-15 containing the homogeneous catalyst **3** (approx. 7-50 mg, depending on the Ru-content and substrate:catalyst ratio) was added. After 24 hours, ^{1}H NMR data were acquired. The conversion and the ratio of macro(mono)cyclization (MMC) to oligomerization (O) were determined by integration of the corresponding signals.

General procedure for the multi-step modification of SBA-15 (GP-5). Refilling: SBA-15 (approx. 10 g) was added to a solution of P123 (40 g) in ethanol (150 mL). The mixture was stirred for 24 hours at room temperature. The suspension was filtered and dried in vacuo at 80 °C for 24 hours. **Selective protection of silanol groups outside the mesopores:** The refilled SBA-15 (approx. 15 g) was treated with hexamethyldisilazane (HMDS, 200 mL) for three hours at room temperature. The mixture was filtered and the selectively protected silica was washed with hexane (500 mL). **Removal of the surfactant:** The surfactant was removed by Soxhlet extraction with ethanol at 140 °C for seven days. **Immobilization of the catalyst:** Refilled, selectively protected, and extracted silica (2 g) was added to a solution of **3** (200 mg) in CH_2Cl_2. For the removal of nitrogen in the pores, vacuum was applied. The suspension was stirred for 7 days at room temperature. Then, the suspension was filtered and the resulting silica containing the immobilized catalyst was washed with CH_2Cl_2 (1000 mL), dried in vacuo at 50 °C for 24 hours, and stored under inert atmosphere at -35 °C.

Pore characterization of the unmodified and modified SBA-15 were carried out *via* Ar sorption measurements (Figures S1-S5), EDX measurements (Figures S6-S7) and solid-state NMR (Figure S8).

Molecular dynamics simulations. The cylindrical mesopore model consisted of a 4.8 nm-diameter pore carved through the (111) face of a β-cristobalite block (8.096 nm × 7.893 nm × 10 nm ($x \times y \times z$)) along the z-direction, following procedures reported previously,[43-44] resulting in 5.55 silanol groups/nm² on the inner pore surface. The cylindrical pore was flanked by two solvent reservoirs with the outer surfaces bearing 4.52 silanol groups/nm². They were grafted uniformly random with 2.70 trimethylsilyl groups/nm² to mimic experimental conditions, where the silanols on the external surface of the SBA-15 silica particles have been shielded. Two systems were simulated, which differed in the surface modification inside the pore: the bare silica surface bearing 5.55 silanol groups/nm² and a DMDMS-modified silica surface with 3.34 DMDMS groups/nm² (leaving 2.21 residual silanol groups/nm²). Each cylindrical pore was then grafted with two catalysts **3**. Both systems were equilibrated with an equimolar mixture of substrate **5** and its MMC product **12** in benzene at 50°C. The number of benzene molecules in the simulation box was $N_{benzene}$ = 4872 for the bare-silica pore and $N_{benzene}$ = 4620 for the DMDMS-modified pore. Each simulation system contained 10 substrate and 10 product molecules corresponding to a 20 mM solution of substrate and product, respectively. Force-field parameters for Si, O, and H atoms of the silica surface were taken from Gulmen and Thompson.[45-46] The GAFF force field was used for substrate, product, and benzene molecules as well as for the surface groups.[47] Catalyst **3** was modeled in its precursor state, using structural parameters from the single-crystal X-ray structure (Figure 2b) and GAFF force field parameters combined with force constants reported by Ahmadi et al.;[48] partial atomic charges were calculated with the DDEC approach.[49] Simulations were run using GROMACS 2016.5.[50] Equilibration was carried out for 50 ns and the spatially-dependent density and diffusion profiles were generated from a 600 ns trajectory.

CONCLUSIONS

We successfully established a biomimetic approach to improve macrocyclization and suppress oligomerization in the RCM-based synthesis of macrocyclic compounds. The method presented here allows for a resilient and generally valid correlation between the size of a substrate (as well as subtle changes thereof) and its propensity to undergo macro(mono)cyclization with a catalyst located inside a silica mesopore of defined shape and size (cylinder diameter). Both pore diameter and hydrodynamic radius of the substrate have been shown to influence macrocyclization selectivity. The extension to a nonpolar inner surface additionally increases macrocyclization selectivity by reducing the pore diameter and facilitating diffusion via decreased adsorption of substrate molecules onto the modified surface. Also, the importance of a pore-selective catalyst immobilization with all catalysts immobilized inside the pores – sufficiently far away from the pore entrances – has been demonstrated. The presented approach allows for substantially higher macrocyclization selectivity and higher substrate concentrations compared to existing procedures. Further improvements can be expected from tailored surface modifications of the pore morphologies, which will help to explore and utilize the full potential of the synergistic effects on macrocyclization selectivity arising from the intrinsic spatial confinement, specific interactions with the surface, local residence times, and average transport rates.

ASSOCIATED CONTENT

Catalyst synthesis, silica surface modification, and macrocyclization reactions, experimental procedures, analysis, full characterization; force field and simulation parameters, analysis of simulated data.

CCDC 1942469 (**3**) contains the supplementary crystallographic data for this paper. These data can be obtained free of charge from the Cambridge Crystallographic Data Centre.

AUTHOR INFORMATION

Corresponding Author

*michael.buchmeiser@ipoc.uni-stuttgart.de

Funding Sources

Financial support by the Deutsche Forschungsgemeinschaft DFG (grant numbers TA 268/11-1 and 358283783 – CRC 1333) and the Ministry of Science, Research, and the Arts Baden-Württemberg is gratefully acknowledged. Simulations were performed on the supercomputer ForHLR I funded by the Ministry of Science, Research, and the Arts Baden-Württemberg and by the Federal Ministry of Education and Research.

ACKNOWLEDGMENT

We thank the Plietker group (Department of Organic Chemistry, University of Stuttgart) for the access to their prep-scale HPLC equipment. We thank Viola Duppel, MPI-FKF, Stuttgart, for the EDX measurements.

ABBREVIATIONS

MMC, macro(mono)cyclization product; O, oligomerization product; DMDMS, dimethyldimethoxysilane; RCM, ring-closing metathesis; ADMET, acyclic diene metathesis; SBA, Santa Barbara Amorphous.

REFERENCES

1. Villar, E. A.; Beglov, D.; Chennamadhavuni, S.; Porco Jr, J. A.; Kozakov, D.; Vajda, S.; Whitty, A., How proteins bind macrocycles. *Nature Chem. Biol.* **2014,** *10*, 723-731.
2. Heinis, C., Drug discovery: tools and rules for macrocycles. *Nature Chem. Biol.* **2014,** *10*, 696-698.
3. Martí-Centelles, V.; Pandey, M. D.; Burguete, M. I.; Luis, S. V., Macrocyclization Reactions: The Importance of Conformational, Configurational, and Template-Induced Preorganization. *Chem. Rev.* **2015,** *115*, 8736–8834.
4. Fu, G. C.; Grubbs, R. H., The application of catalytic ring-closing olefin metathesis to the synthesis of unsaturated oxygen heterocycles. *J. Am. Chem. Soc.* **1992,** *114*, 5426-5427.
5. Grubbs, R. H.; Miller, S. J.; Fu, G. C., Ring-closing metathesis and related processes in organic synthesis. *Acc. Chem. Res.* **1995,** *28*, 446-452.
6. Lee, C. W.; Grubbs, R. H., Formation of macrocycles via ring-closing olefin metathesis. *J. Org. Chem.* **2001,** *66*, 7155-7158.
7. Sattely, E. S.; Cortez, G. A.; Moebius, D. C.; Schrock, R. R.; Hoveyda, A. H., Enantioselective synthesis of cyclic amides and amines through Mo-catalyzed asymmetric ring-closing metathesis. *J. Am. Chem. Soc.* **2005,** *127*, 8526-8533.
8. Lee, A.-L.; Malcolmson, S. J.; Puglisi, A.; Schrock, R. R.; Hoveyda, A. H., Enantioselective synthesis of cyclic enol ethers and all-carbon quaternary stereogenic centers through catalytic asymmetric ring-closing metathesis. *J. Am. Chem. Soc.* **2006,** *128*, 5153-5157.
9. Seiders, T. J.; Ward, D. W.; Grubbs, R. H., Enantioselective ruthenium-catalyzed ring-closing metathesis. *Org. Lett.* **2001,** *3*, 3225-3228.
10. Fürstner, A., Olefin Metathesis and Beyond. *Angew. Chem. Int. Ed.* **2000,** *39*, 3012-3043.
11. Nicolaou, K. C.; Bulger, P. G.; Sarlah, D., Palladium-Catalyzed Cross-Coupling Reactions in Total Synthesis. *Angew. Chem. Int. Ed.* **2005,** *44*, 4442-4489.
12. Marx, V. M.; Herbert, M. B.; Keitz, B. K.; Grubbs, R. H., Stereoselective Access to Z and E Macrocycles by Ruthenium-Catalyzed Z-Selective Ring-Closing Metathesis and Ethenolysis. *J. Am. Chem. Soc.* **2013,** *135*, 94-97.
13. Alexander, J. B.; La, D. S.; Cefalo, D. R.; Hoveyda, A. H.; Schrock, R. R., Catalytic Enantioselective Ring-Closing Metathesis by a Chiral Biphen-Mo Complex. *J. Am. Chem. Soc.* **1998,** *120*, 4041-4042.
14. Zhang, H.; Yu, E. C.; Torker, S.; Schrock, R. R.; Hoveyda, A. H., Preparation of Macrocyclic Z-Enoates and (E,Z)- or (Z,E)-Dienoates through Catalytic Stereoselective

Ring-Closing Metathesis. *J. Am. Chem. Soc.* **2014,** *136*, 16493-16496.

15. Shen, X.; Nguyen, T. T.; Koh, M. J.; Xu, D.; Speed, A. W. H.; Schrock, R. R.; Hoveyda, A. H., Kinetically E-selective macrocyclic ring-closing metathesis. *Nature* **2017,** *541*, 380-385.

16. Conrad, J. C.; Eelman, M. D.; Duarte Silva, J. A.; Monfette, S.; Parnas, H. H.; Snelgrove, J. L.; Fogg, D. E., Oligomers as Intermediates in Ring-Closing Metathesis. *J. Am. Chem. Soc.* **2007,** *129*, 1024-1025.

17. Monfette, S.; Fogg, D. E., Equilibrium Ring-Closing Metathesis. *Chem. Rev.* **2009,** *109*, 3783-3816.

18. Fürstner, A.; Langemann, K., Conformationally Unbiased Macrocyclization Reactions by Ring Closing Metathesis. *J. Org. Chem.* **1996,** *61*, 3942-3943.

19. Evano, G.; Schaus, J. V.; Panek, J. S., A Convergent Synthesis of the Macrocyclic Core of Cytotrienins: Application of RCM for Macrocyclization. *Org. Lett.* **2004,** *6*, 525-528.

20. Bertinato, P.; Sorensen, E. J.; Meng, D.; Danishefsky, S. J., Studies toward a Synthesis of Epothilone A: Stereocontrolled Assembly of the Acyl Region and Models for Macrocyclization. *J. Org. Chem.* **1996,** *61*, 8000-8001.

21. Galli, C., "Cesium Ion Effect" and macrocyclization. A critical review. *Org. Prep. Proced. Int.* **1992,** *24*, 285-307.

22. Marsella, M. J.; Maynard, H. D.; Grubbs, R. H., Template-Directed Ring-Closing Metathesis: Synthesis and Polymerization of Unsatuared Crown Ether Analogs. *Angew. Chem. Int. Ed.* **1997,** *36*, 1101-1103.

23. Cantrill, S. J.; Grubbs, R. H.; Lanari, D.; Leung, K. C. F.; Nelson, A.; Poulin-Kerstien, K. G.; Smidt, S. P.; Stoddart, J. F.; Tirrell, D. A., Template-Directed Olefin Cross Metathesis. *Org. Lett.* **2005,** *7*, 4213-4216.

24. Higman, C. S.; Nascimento, D. L.; Ireland, B. J.; Audörsch, S.; Bailey, G. A.; McDonald, R.; Fogg, D. E., Chelate-Assisted Ring-Closing Metathesis: A Strategy for Accelerating Macrocyclization at Ambient Temperatures. *J. Am. Chem. Soc.* **2018,** *140*, 1604-1607.

25. Sytniczuk, A.; Dąbrowski, M.; Banach, Ł.; Urban, M.; Czarnocka-Śniadała, S.; Milewski, M.; Kajetanowicz, A.; Grela, K., At Long Last: Olefin Metathesis Macrocyclization at High Concentration. *J. Am. Chem. Soc.* **2018,** *140*, 8895-8901.

26. Buchmeiser, M. R., Polymer-Supported Well-Defined Metathesis Catalysts. *Chem. Rev.* **2009,** *109*, 303-321.

27. Jee, J.-E.; Cheong, J. L.; Lim, J.; Chen, C.; Hong, S. H.; Lee, S. S., Highly Selective Macrocycle Formation by Metathesis Catalysts Fixation in Nanopores. *J. Org. Chem.* **2013,** *78*, 3048-3056.

28. Lim, J.; Lee, S. S.; Riduan, S. N.; Ying, J. Y., Mesocellular Foam-Supported Catalysts: Enhanced Activity and Recyclability for Ring-Closing Metathesis. *Adv. Synth. Catal.* **2007,** *349*, 1066-1076.

29. Buchmeiser, M. R., *Immobilization of Metathesis Catalysts*. In: "Olefin Metathesis - Theory and Praxis (Grela, K., Ed.) John Wiley & Sons: 2014; p 495-514..

30. Bru, M.; Dehn, R.; Teles, J. H.; Deuerlein, S.; Danz, M.; Müller, I. B.; Limbach, M., Ruthenium Carbenes Supported on Mesoporous Silicas as Highly Active and Selective Hybrid Catalysts for Olefin Metathesis Reactions under Continuous Flow. *Chem. Eur. J.* **2013,** *19*, 11661–11671.

31. Wu, N.-W.; Petsalakis, I. D.; Theodorakopoulos, G.; Yu, Y.; Rebek, J., Cavitands as containers for α,ω-dienes and chaperones for olefin metathesis. *Angew. Chem. Int. Ed.* **2018,** *57*, 15091-15095.

32. Zhao, D.; Feng, J.; Huo, Q.; Melosh, N.; Fredrickson, G. H.; Chmelka, B. F.; Stucky, G. D., Triblock Copolymer Syntheses of Mesoporous Silica with Periodic 50 to 300 Angstrom Pores. *Science* **1998,** *279*, 548.

33. Soler-Illia, G. J. d. A. A.; Crepaldi, E. L.; Grosso, D.; Sanchez, C., Block copolymer-templated mesoporous oxides. *Curr. Opin. Colloid Interface Sci.* **2003,** *8*, 109-126.

34. Ward, T. R., Artificial Metalloenzymes Based on the Biotin–Avidin Technology: Enantioselective Catalysis and Beyond. *Acc. Chem. Res.* **2011,** *44*, 47-57.

35. Heinisch, T.; Ward, T. R., Artificial Metalloenzymes Based on the Biotin–Streptavidin Technology: Challenges and Opportunities. *Acc. Chem. Res.* **2016,** *49*, 1711-1721.

36. Schwizer, F.; Okamoto, Y.; Heinisch, T.; Gu, Y.; Pellizzoni, M. M.; Lebrun, V.; Reuter, R.; Köhler, V.; Lewis, J. C.; Ward, T. R., Artificial Metalloenzymes: Reaction Scope and Optimization Strategies. *Chem. Rev.* **2018,** *118*, 142-231.

37. Reich, S.-J.; Svidrytski, A.; Höltzel, A.; Florek, J.; Kleitz, F.; Wang, W.; Kübel, C.; Hlushkou, D.; Tallarek, U., Hindered Diffusion in Ordered Mesoporous Silicas: Insights from Pore-Scale Simulations in Physical Reconstructions of SBA-15 and KIT-6 Silica. *J. Phys. Chem. C* **2018,** *122*, 12350-12361.

38. Webb, J. D.; Seki, T.; Goldston, J. F.; Pruski, M.; Crudden, C. M., Selective functionalization of the mesopores of SBA-15. *Micropor. Mesopor. Mat.* **2015,** *203*, 123-131.

39. Dias, E. L.; Nguyen, S. T.; Grubbs, R. H., Well-Defined Ruthenium Olefin Metathesis Catalysts: Mechanism and Activity. *J. Am. Chem. Soc.* **1997,** *119*, 3887-3897.

40. Hérisson, J.-L.; Chauvin, Y., Catalyse de transformation des oléfines par les complexes du tungstène. II. Télomérisation des oléfines cycliques en présence d'oléfines acycliques. *Makromol. Chem.* **1971,** *141*, 161-176.

41. Adlhart, C.; Chen, P., Mechanism and Activity of Ruthenium Olefin Metathesis Catalysts: The Role of Ligands and Substrates from a Theoretical Perspective. *J. Am. Chem. Soc.* **2004,** *126*, 3496-3510.

42. Romero, P. E.; Piers, W. E., Direct Observation of a 14-Electron Ruthenacyclobutane Relevant to Olefin Metathesis. *J. Am. Chem. Soc.* **2005,** *127*, 5032-5033.

43. Coasne, B.; Di Renzo, F.; Galarneau, A.; Pellenq, R. J. M., Adsorption of Simple Fluid on Silica Surface and Nanopore: Effect of Surface Chemistry and Pore Shape. *Langmuir* **2008,** *24*, 7285-7293.

44. Melnikov, S. M.; Höltzel, A.; Seidel-Morgenstern, A.; Tallarek, U., A Molecular Dynamics Study on the Partitioning Mechanism in Hydrophilic Interaction Chromatography. *Angew. Chem. Int. Ed.* **2012,** *51*, 6251-6254.

45. Gulmen, T. S.; Thompson, W. H., Testing a Two-State Model of Nanoconfined Liquids: Conformational Equilibrium of Ethylene Glycol in Amorphous Silica Pores. *Langmuir* **2006,** *22*, 10919-10923.

46. Steenbergen, K. G.; Kern, J. L.; Wang, Z.; Thompson, W. H.; Laird, B. B., Tunability of Gas-Expanded Liquids under Confinement: Phase Equilibrium and Transport Properties of Ethylene-Expanded Methanol in Mesoporous Silica. *J. Phys. Chem. C* **2016,** *120*, 5010-5019.

47. Wang, J.; Wang, W.; Kollman, P. A.; Case, D. A., Automatic atom type and bond type perception in molecular mechanical calculations. *J. Mol. Graph. Model.* **2006,** *25*, 247-260.

48. Ahmadi, A.; McBride, C.; Freire, J. J.; Kajetanowicz, A.; Czaban, J.; Grela, K., Force Field Parametrization and Molecular Dynamics Simulation of Flexible POSS-Linked (NHC; Phosphine) Ru Catalytic Complexes. *J. Phys. Chem. A* **2011,** *115*, 12017-12024.

49. Manz, T. A.; Limas, N. G., Introducing DDEC6 atomic population analysis: part 1. Charge partitioning theory and methodology. *RSC Advances* **2016,** *6*, 47771-47801.

50. Abraham, M. J.; Murtola, T.; Schulz, R.; Páll, S.; Smith, J. C.; Hess, B.; Lindahl, E., GROMACS: High performance molecular simulations through multi-level parallelism from laptops to supercomputers. *SoftwareX* **2015,** *1-2*, 19-25.

Table of Contents